Biochemical and Biophysical Research Communications 464 (2015) 622–628

Contents lists available at ScienceDirect

Biochemical and Biophysical Research Communications

journal homepage: www.elsevier.com/locate/ybbrc

Insights into unknown foreign ligand in copper nitrite reductase

Yohta Fukuda [a, 1], Ka Man Tse [b], Yuji Kado [a, b], Eiichi Mizohata [a], Hiroyoshi Matsumura [a, 2], Tsuyoshi Inoue [a, *]

[a] Department of Applied Chemistry, Graduate School of Engineering, Osaka University, 2-1 Yamadaoka, Suita, Osaka 565-0871, Japan
[b] Interdisciplinary Program for Biomedical Sciences, Institute for Academic Initiatives, Osaka University, 1-1 Yamadaoka, Suita, Osaka 565-0871, Japan

ARTICLE INFO

Article history:
Received 26 June 2015
Accepted 5 July 2015
Available online 9 July 2015

Keywords:
X-ray crystallography
Structural biology
Copper
Enzyme

ABSTRACT

Bifunctional copper nitrite reductase (CuNIR) catalyzes nitrite reduction to nitric oxide and dioxygen reduction to hydrogen peroxide. In contrast to the well-researched nitrite reduction mechanism, the oxygen reduction mechanism in CuNIR has been totally unknown, because mononuclear copper–oxygen complexes decompose so readily that their visualization has been challenging. Here, we provide spectroscopic evidence that a foreign ligand binds to the catalytic copper (T2Cu) site of CuNIR, and determine CuNIR structures displaying a diatomic molecule on T2Cu. This unknown ligand can be interpreted as dioxygen and may provide insights into the oxygen reduction mechanism of CuNIR.

1. Introduction

In the nitrogen cycle, nitrogen oxides are reduced to gaseous dinitrogen in a stepwise manner ($NO_3^- \rightarrow NO_2^- \rightarrow NO \rightarrow N_2O \rightarrow N_2$) [1]. This process, denitrification, is conducted by microorganisms and coupled with their anaerobic respiratory systems. Nitrite reduction to nitric oxide ($NO_2^- + e^- + 2H^+ \rightarrow NO + H_2O$) is the key step in denitrification. In some organisms, the reaction is catalyzed by copper nitrite reductase (CuNIR), which is composed of three monomeric units containing two copper sites: type 1 Cu (T1Cu) and type 2 Cu (T2Cu) [2–5]. The T1Cu site, coordinated by His95, His143, Cys135, and Met148 [the numbers of residues refer to the *Geobacillus thermodenitrificans* CuNIR (*Gt*NIR) sequence], receives an electron from electron-donor proteins. The received electron is subsequently transferred to the catalytic T2Cu site through juxtaposed Cys135 and His134, which are the ligands to T1Cu and T2Cu, respectively. The T2Cu atom is coordinated by His100, His134, and His294 whereby His294 comes from the adjacent monomer. In the resting state, the nitrite binding position on the T2Cu atom is occupied by water.

Typical CuNIRs can also catalyze the two-electron reduction of dioxygen to hydrogen peroxide, which degrades CuNIR itself [6–8]. The T2Cu site in CuNIR is similar to the catalytic site of Zn,Cu superoxide dismutase (Zn,Cu-SOD) [9,10] and shows SOD activity [10,11]. These facts indicate that the T2Cu site in CuNIR has a potential ability as a dioxygen binding site. However, while the mechanism of nitrite reduction by CuNIR has been extensively studied by determining crystal structures of CuNIR in complex with NO_2^- and NO [12,13], the detailed reactions involved in oxygen species has been unexplored because mononuclear copper-dioxygen complexes decompose so readily that their visualization is difficult.

In a previous study, we determined a crystal structure of *Gt*NIR, in which T2Cu was coordinated by a chloride ion contained in the purification buffer [14]. Therefore, our original motivation for this study had been to obtain a chloride-free structure of *Gt*NIR. However, we unexpectedly found a diatomic molecule on T2Cu in the chloride-free form. Because it can be interpreted as dioxygen and may provide insights into the oxygen reduction mechanism in CuNIR, here we want to report the detail.

Abbreviations: CuNIR, copper nitrite reductase; T1Cu, type 1 copper; T2Cu, type 2 copper; *Gt*NIR, *Geobacillus thermodenitrificans* copper nitrite reductase; *Ne*NIR, *Nitrosomonas europaea* copper nitrite reductase; *Af*NIR, *Alcaligenes faecalis* copper nitrite reductase; *Ax*NIR, *Achromobacter xylosoxidans* copper nitrite reductase; *Ac*NIR, *Achromobacter cycloclastes* copper nitrite reductase; MPD, 2-methyl-2,4-pentanediol; Tris, tris(hydroxymethyl)aminomethane; MES, 2-(N-morpholino) ethanesulfonic acid; HEPES, N-2-hydroxyethylpiperazine-N-2-ethanesulfonic acid; WT, wild type; Zn,Cu-SOD, Zn,Cu superoxide dismutase; LMCT, ligand-to-metal charge transfer.

* Corresponding author.
E-mail address: inouet@chem.eng.osaka-u.ac.jp (T. Inoue).
[1] Present address: Department of Biochemistry and Molecular Biophysics, Columbia University, 650 W 168 Street, NY 10032, USA.
[2] Present address: Department of Biotechnology, College of Life Sciences, Ritsumeikan University, 1-1-1 Noji-higashi, Kusatsu Shiga 525-8577, Japan.

http://dx.doi.org/10.1016/j.bbrc.2015.07.025
0006-291X/

2. Materials and methods

2.1. Expression, purification, and crystallization of wild type (WT) and an H294M mutant of GtNIR

Preparation of WT *Gt*NIR was performed as described previously [14] with following modifications. HEPES buffer was used instead of Tris–HCl buffer in order to prevent chloride ions from binding to T2Cu. Additionally, $(NH_4)_2SO_4$ instead of NaCl was used to elute proteins from an anion exchange column. Crystallization was performed as described previously [14]. Crystals were soaked in the cryo-solution containing 0.1 M sodium acetate buffer pH 4.5, 5.5% (w/v) polyethylene glycol 4000, and 35% (v/v) 2-methyl-2,4-pentanediol (MPD) and flash-cooled by immersion in liquid nitrogen prior to data collection.

We made a *Gt*NIR mutant, in which T2Cu ligand His294 is replaced by methionine. The forward and reverse primers for the mutation were 5′-TCCGATCGTTACTATGCAGTTTAATCATGC-3′ and 5′-GCATGATTAAACTGCATAGTAACGATCGGA-3′, respectively. The sequence of the mutant plasmid (pET22b) was confirmed by DNA sequencing. The mutant was overexpressed, purified, and crystallized using the same method as that for the WT protein.

2.2. Oxygen reduction assay

The *o*-dianisidine (3,3′-dimethoxybenzidine dihydrochloride) dependent assay was performed as described previously [8,15]. A saturated *o*-dianisidine solution was prepared by stirring excess *o*-dianisidine in 80 mM MES-HEPES buffer, pH 7.0 overnight. Insoluble *o*-dianisidine powders were eliminated by filtering with a 0.22 μm filter. The reaction was initiated by adding WT or the H294M mutant of *Gt*NIR. Final concentration of the enzymes was 1.6 μM. Oxidation of *o*-dianisidine was monitored by the increase in absorbance at 460 nm (11,300 M^{-1} cm^{-1}) with a UV-2550 UV–vis spectrophotometer (Shimadzu, Kyoto, Japan). The measurement temperature was kept at 25 °C by a TCC-240A temperature controller (Shimadzu). The assay was performed three times for WT and the H294M mutant, respectively.

2.3. Microspectroscopy

The UV–vis spectra of a *Gt*NIR crystal (~0.3 × 0.4 × 0.1 mm) were measured using a microspectrophotometer connected with an X-ray diffractometer installed at beamline BL38B1 at SPring-8 (Hyogo, Japan) [16]. All UV–vis microspectrum data were measured in a 100 K cryostream and were collected four times to increase signal to noise ratios. The spectra were recorded every 45 s X-ray irradiation. The X-ray dose for 45 s irradiation, which was calculated with RADDOSE [17], was 0.041 MGy. Differences of UV–vis absorption due to different crystal thicknesses were avoided by fixing the direction of the crystal and the measurement position for each measurement. The UV–vis spectra only of the cryo-solution were measured with the same cryoloop as that used for the *Gt*NIR crystal.

2.4. Crystal structure determination

The dataset for one of the two WT crystals (WT-OXY1) was collected at 100 K on beamline BL38B1 at SPring-8 using an ADSC Quantum 315 CCD detector (Area Detector Systems Co., CA, USA). This is the same crystal as the crystal that was used in the microspectroscopic analysis described above. The higher-resolution dataset for the other *Gt*NIR crystal (WT-OXY2) grown under the same condition as WT-OXY1 was collected at 100 K on beamline BL1A at Photon Factory (Ibaraki, Japan) using a Pilatus 2M-F detector (DECTRIS Ltd., Baden, Switzerland). Total X-ray doses for WT-OXY1 and WT-OXY2 were ~0.16 and ~0.18 MGy, respectively. The HKL2000 package [18] was used to reduce, integrate and scale the collected data. The phases were determined by molecular replacement using the program MOLREP [19] from the CCP4 suite [20]. A monomeric subunit of *Gt*NIR (PDB code 4ZK8) was used as the search model. The resulting models were refined by REFMAC5 [21]. Manual model building was performed using COOT [22]. The final models were checked for stereochemical quality using MolProbity [23]. Data collection and refinement statistics are summarized in Table 1.

The diffraction dataset for a H294M crystal was collected at 100 K on beamline BL38B1 at SPring-8 using the ADSC Quantum 315 CCD detector. The dataset was reduced, integrated and scaled with the HKL2000 package. Phasing was performed by molecular replacement using MolRep. The monomeric subunit of WT *Gt*NIR (PDB code 4ZK8) was used as the search model. The resulting model was refined with Refmac5. Manual model building was carried out using COOT through the refinement process. The final model was checked for stereochemical quality using MolProbity. Data collection and refinement statistics are summarized in Table 1.

3. Results

3.1. Oxygen reduction assay

o-dianisidine and dioxygen can be an electron donor and a terminal electron acceptor in the reaction system, respectively [8,15]. Addition of WT *Gt*NIR or the H294M mutant to the saturated *o*-dianisidine solution caused a jump of absorbance at 460 nm (Fig. 1A), because oxidized *Gt*NIR has an absorption peak at around 450 nm (Fig. 1B). Addition of WT *Gt*NIR showed a linear increase in absorbance (Fig. 1A). Conversely, the H294M mutant did not show the oxygen reduction ability (Fig. 1A). The dioxygen reduction rate of WT *Gt*NIR was $2.4 \times 10^{-4} \pm 1.3 \times 10^{-5}$ s^{-1}, which is about 17 times slower than 4.2×10^{-3} s^{-1} of CuNIR from mesophilic *Alcaligenes faecalis* (*Af*NIR) [8].

3.2. Microspectroscopic analysis

The UV–vis spectrum of the *Gt*NIR crystal before X-ray irradiation (red line in Fig. 1C) shows absorption bands with peaks at around 450 and 600 nm, which correspond to peaks observed in the solution UV–vis spectrum of aerobically oxidized *Gt*NIR (Fig. 1B). These bands are derived from ligand-to-metal charge transfer (LMCT) transitions from the sulfur atom of Cys135 to oxidized (Cu^{2+}) T1Cu [24]. Moreover, weak absorption originating from a *d*–*d* transition of Cu^{2+} was observed between 650 and 750 nm (Fig. 1C).

Synchrotron X-ray beams is known to cause reduction of the metal sites in metalloproteins [25,26]. As the dose of X-ray increased, the intensities of absorption at around 450 and 600 nm became weaker (Fig. 1C and D). The band of the *d*–*d* transition decreased, too. Conversely, the absorption intensity between 300 and 400 nm increased during exposure of the crystal to X-ray (Fig. 1C and D). These changes occurred sequentially. In other words, the decreases of absorption, derived from oxidized copper sites (at 450, 600, and ~700 nm), were first recorded and then the increase of absorption between 300 and 400 nm became conspicuous (Fig. 1C and D). The UV–vis spectrum between 300 and 400 nm only of the crystallization buffer was not significantly changed by X-ray irradiation (Fig. S1).

Table 1
Data collection and refinement statistics.

Name (PDB code)	WT-OXY1 (3WNI)	WT-OXY2 (3WNJ)	H294M (3X1F)
Data collection			
Synchrotron beamline	SPring-8 BL38B1	PF BL1A	SPring-8 BL38B1
Detector	Quantum 315	Pilatus 2M	Quantum 315
Wavelength (Å)[a]	0.75000	0.96000	0.78000
Oscillation angle (°)	1.0	1.0	1.0
Exposure per image (s)	1.5	2.0	1.5
Total images	120	120	120
Space group	*H*3 (*R*3)	*H*3 (*R*3)	*H*3 (*R*3)
Unit cell $a = b$, c (Å)	115.0, 84.5	114.9, 84.0	115.0, 84.1
Resolution range (Å)	50.0–1.50 (1.55–1.50)[a]	100.0–1.20 (1.22–1.20)	50.0–1.35 (1.39–1.35)
R_{sym} (%)[b]	10.3 (31.0)	7.5 (26.3)	10.5 (26.9)
Completeness (%)	97.0 (99.7)	92.1 (96.8)	88.2 (87.6)
Unique reflections	64,781 (6639)	120,357 (6323)	80,403 (4040)
$\langle I \rangle / \langle \sigma (I) \rangle$	14.3 (2.9)	16.6 (3.0)	15.3 (2.5)
Redundancy	2.9 (2.8)	3.5 (3.3)	3.6 (3.5)
Refinement			
Resolution range (Å)	42.9–1.90	28.7–1.20	18.4–1.35
R_{work} (%)[c]/R_{free} (%)[d]	10.8/14.9	12.0/14.6	9.19/11.5
RMSD bond length (Å)	0.026	0.031	0.019
RMSD bond angle (°)	2.198	2.439	2.02
Average B (Å^2)	15.7	15.6	14.2
No. of protein atoms	2446	2600	2493
No. of heterogen atoms	24	66	49
No. of water molecules	379	396	390
Ramachandran (%)			
Favored	98.3	99.0	97.8
Allowed	1.7	1.0	2.2
Outliers	0	0	0

[a] Values in parentheses are for the highest-resolution shell.
[b] R_{sym} is calculated as $\Sigma_{hkl}\Sigma_i|I_i(hkl) - \langle I(hkl)\rangle|/\Sigma_{hkl}\Sigma_i I(hkl)$, where $I_i(hkl)$ is the intensity of an individual measurement of the reflection with Miller indices *hkl* and $\langle I(hkl)\rangle$ is the average intensity from multiple observations.
[c] $R_{work} = \Sigma_{hkl}||F_{obs}| - |F_{calc}||/\Sigma_{hkl}|F_{obs}|$, where F_{obs} and F_{calc} are the observed and calculated structure-factor amplitudes, respectively.
[d] The free *R* factor, R_{free}, is computed in the same manner as R_{work} but using only a small set (5%) of randomly chosen intensities that were not used in the refinement of the model.

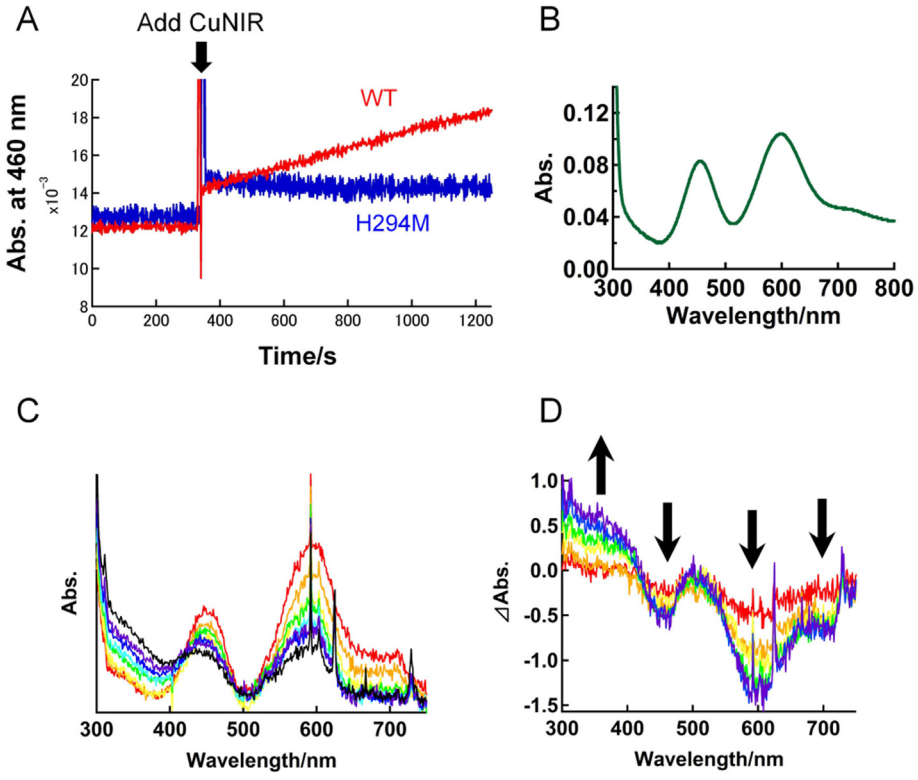

Fig. 1. Spectroscopic data. (A) Oxygen reduction assay. One of the three measurements is illustrated. (B) Solution UV–vis spectrum of *Gt*NIR recorded at room temperature in 40 mM acetate buffer pH 4.5. (C) X-ray-induced reduction of the crystal of *Gt*NIR using 0.75 Å radiation. The red line shows the spectrum recorded before X-ray irradiation. The spectra from orange to purple are recorded every 45 s. The black line illustrates the spectrum recorded after 9 min exposure. (D) The difference spectra of the *Gt*NIR crystal. The significant changes in intensity of spectra are shown by black arrows. (For interpretation of the references to color in this figure legend, the reader is referred to the web version of this article.)

3.3. Crystal structures of WT GtNIR

The crystal structures of WT-OXY1 and WT-OXY2 were determined at 1.50 and 1.20 Å resolution, respectively. In both F_o-F_c electron density maps for WT-OXY1 and WT-OXY2, ellipsoidal electron density was observed above the T2Cu atom. When one water molecule was assigned at the position, positive electron density peaks remained. When two water molecules were assigned, they were too close to be present at the same time. The electron density could best be modeled as a diatomic molecule (Fig. 2A and Fig. S2A). We assigned dioxygen because T2Cu in CuNIR can interact with it. In both WT-OXY1 and WT-OXY2 cases, the dioxygen molecules could have 80% occupancy. Binding modes of them were more side-on than end-on because the distances between the oxygen atoms and the copper atom were 2.35 and 1.96 Å (WT-OXY1) or 2.40 and 2.13 Å (WT-OXY2), respectively. Because NO can assume the side-on binding mode in CuNIR [12,13,27], the side-on diatomic molecule on T2Cu is reasonable. The detailed coordination geometries are summarized in Table 2. In both WT-OXY1 and WT-OXY2 structures, the water molecule (Wat0) with 20% occupancy was observed next to the oxygen molecule (Fig. 2A and Fig. S2A). In the WT-OXY2 structure, water molecule (Wat0′) with 20% occupancy was present at the same position as the O_{distal} atom (the farther atom from T2Cu) of the oxygen molecule (Fig. S2B). The bond lengths of dioxygen, which were not restrained in refinement, were 1.25 and 1.26 Å in the WT-OXY1 and WT-OXY2 structures, respectively. The F_o–F_c maps for WT-OXY1 and WT-OXY2 calculated with the dioxygen model and ligand water showed no significant positive or negative electron density at the both ends and the middle of the dioxygen molecule (Fig. S2B), meaning that the O–O distances were not biased by a standard dictionary in the refinement software. Both O_{distal} and $O_{proximal}$ atoms of dioxygen can interact with the $C^{\gamma 2}$ atom of Val246 through van der Waals contacts (Fig. 2C), which may make the ligand side-on. The geometries of the T1Cu and T2Cu sites of the WT structures were summarized in Table 2.

3.4. Crystal structure of the H294M mutant

The structure of the H294M mutant was determined at 1.35 Å resolution. The amino-acid substitution of the ligand to the T2Cu center caused no perturbation of the overall structure (C^{α} RMSD

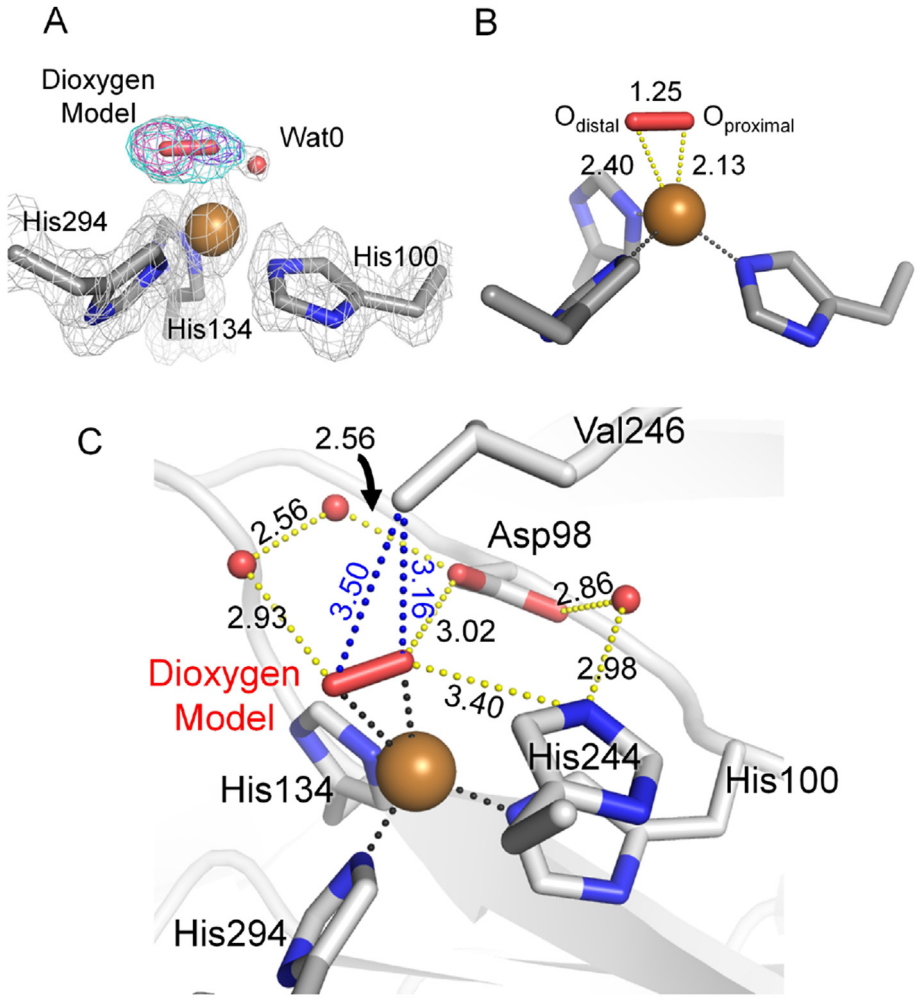

Fig. 2. Dioxygen model in *Gt*NIR (WT-OXY2). (A) Electron density maps around the T2Cu site. The $2F_o$-F_c map (1.5 σ) is represented by a gray mesh. Difference omit maps leaving out both oxygen atoms (cyan mesh) and either the distal oxygen (magenta mesh) or the proximal oxygen (purple mesh) are shown contoured at 8.0 σ. (B) Coordination geometry of the oxygen species. Bonds between T2Cu (brown sphere) and protein ligands are shown as dotted black lines. Bonds between T2Cu and dioxygen are shown as dotted yellow lines. Carbon, oxygen and nitrogen atoms are colored gray, red, and blue, respectively. (C) Environment around the T2Cu site of *Gt*NIR (WT-OXY2). Hydrogen bonds and van der Waals contacts around the dioxygen molecule are illustrated by dotted yellow and blue lines, respectively. Coordination bonds are shown as dotted black lines. Distances are shown in Å. (For interpretation of the references to color in this figure legend, the reader is referred to the web version of this article.)

Table 2
Copper site geometries.

Parameter	WT-OXY1	WT-OXY2	H294M
I. Type 1 Cu–ligand distances (Å)			
T1Cu–H95N$^{\delta1}$	2.04	2.03	2.04
T1Cu–C135S$^{\gamma}$	2.16	2.18	2.19
T1Cu–H143N$^{\delta1}$	1.99	2.09	1.99
T1Cu–M148S$^{\delta}$	2.63	2.61	2.58
II. Type 2 Cu–ligand distances (Å)			
T2Cu–H100N$^{\varepsilon2}$	1.97	1.92	2.04
T2Cu–H134N$^{\varepsilon2}$	2.03	2.03	2.08
T2Cu–H294N$^{\varepsilon2}$/M294S$^{\delta}$	2.02	1.98	2.28
T2Cu–Wat0 (Wat0′)	2.23	2.19 (2.21)	2.18
T2Cu–O$_{distal}$	2.35	2.40	n/a
T2Cu–O$_{proximal}$	1.96	2.13	n/a
O–O distance	1.25	1.26	n/a
III. Angles (°)			
T2Cu–O$_{proximal}$–O$_{distal}$	91.1	86.7	n/a

between H294M and WT-OXY1 or WT-OXY2 was 0.07 Å) and the geometry of the T1Cu site (Fig. 3A and Table 2). Conversely, the T2Cu center showed obvious geometrical changes (Fig. 3B and C). In the WT structure, three histidyl residues bound to the T2Cu atom at almost equal distances (~2.0 Å) whereas in the H294M mutant, the sulfur atom of methionine was farther from the T2Cu atom (2.28 Å) than the two N$^{\varepsilon2}$ atoms of His100 and His134 (2.04 and 2.08 Å, respectively). In addition, only one water molecule (Wat0) was found on the T2Cu atom (Fig. 3B). An acetate molecule was located near the T2Cu site to form hydrogen bonds with the O$^{\delta2}$ atom of Asp98 and Wat0 (Fig. 3B) whereas in the WT *Gt*NIR structures, two water molecules are located at the same positions as the carboxyl oxygen atoms of the acetate molecule. The geometries of the T1Cu and T2Cu sites of the H294M mutant are summarized in Table 2.

4. Discussion

The intensities of the LMCT and *d*–*d* transition bands of the *Gt*NIR crystal decreased during X-ray irradiation (Fig. 1C and D), which demonstrated that the T1Cu site changed from an oxidized state to a reduced state [24,28]. However, the rate of the decreases in intensities of bands gradually became slow, and the T1Cu site was not completely reduced after 9 min X-ray irradiation (black line in Fig. 1C). This may be because electrons flowed from the T1Cu site to the T2Cu site and hence a certain amount of the T1Cu atoms in the crystal was re-oxidized. Another spectral change was the appearing of a shoulder between 300 and 400 nm. Although a cryo-solution containing MPD shows the increase in absorption between 240 and 350 nm when the X-ray exposure time is long [16], there was no spectral change in the spectrum of the cryo-solution within 4.5 min (Fig. S1). These facts implied that an unknown ligand bound to the T2Cu atom and caused an LMCT transition. We speculated that it was a side-on dioxygen species because CuNIR can interact with dioxygen and because a side-on superoxo-copper(II) complex has an LMCT absorption band at 352 nm [29]. Many other copper(II)-dioxygen complexes show absorption bands between 300 and 400 nm [30,31].

The crystal structures support our hypothesis, because the ellipsoidal electron density above the WT T2Cu site exhibited presence of a diatomic molecule (Fig. 2A and Fig. S2A), while a spherical electron density, which was assigned to a water molecule, was observed in the H294M mutant (Fig. 3B), which showed no dioxygen reduction activity. The diatomic molecule could not be N_2, CO, or NO because they were only present in trace amounts in the used buffer. Considering that CuNIR functions as oxygen reductase, it is probable that the ligand is dioxygen species. Although the high occupancy of the diatomic molecule in WT-OXY1 is apparently incompatible with the result of microspectroscopic analysis (Fig. 1C), there is no quantitative linear relationship between the microspectroscopic data and the X-ray diffraction data because the paths and beam sizes of UV–vis rays and X-rays in our experimental system were different. The modeled dioxygen species in WT-OXY1 and WT-OXY2 had bond distances refined to values of 1.26 and 1.25 Å, respectively, which were compatible with typical O–O distances of neutral dioxygen or superoxide anion (1.2–1.3 Å) but not with that of peroxide (1.4–1.5 Å) [32].

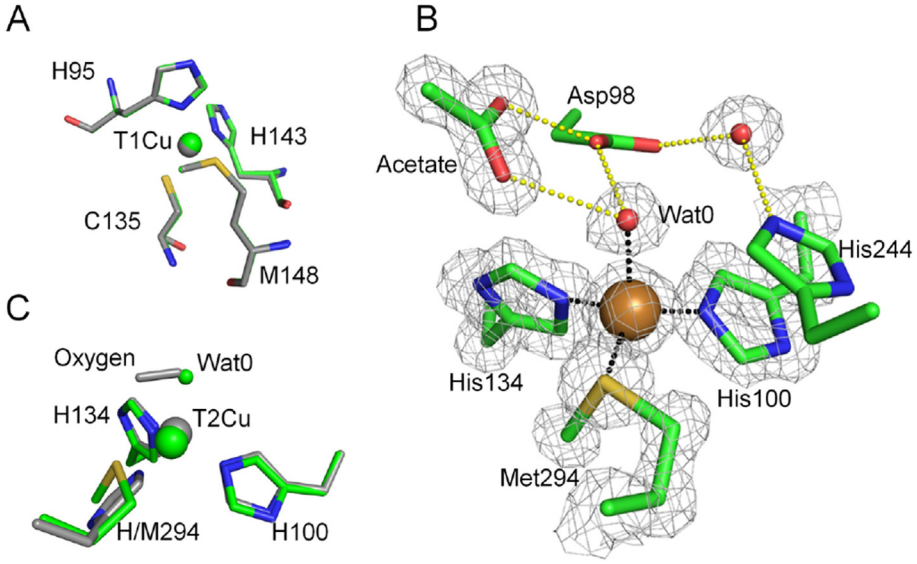

Fig. 3. The copper sites in the H294M mutant. (A) Superimposition of the T1Cu site in the H294M mutant (green) on that in WT (gray). The copper atoms are shown as spheres. (B) The detailed structure of the T2Cu site in the H294M mutant. The copper ions and the water molecules are shown as brown and red spheres, respectively. Carbon, oxygen, nitrogen, and sulfur atoms are shown in green, red, blue, and yellow, respectively. Coordination bonds (black) and hydrogen bonds (yellow) are shown as dotted lines. The $2F_o$–F_c map (1.5 σ) is represented by gray meshes. (C) Superimposition of the T2Cu site in the H294M mutant (green) on that in WT (gray). The copper atoms and water molecule are shown as large and small spheres, respectively. Dioxygen in the WT structure is represented by the gray stick model. (For interpretation of the references to color in this figure legend, the reader is referred to the web version of this article.)

The oxygen reduction rate of *Gt*NIR was slower than that of *Af*NIR. This is probably because CuNIR from themophilic bacterium has a rigid catalytic site and the catalytic ability at room temperature is low [14,33]. This slow oxygen reduction rate of *Gt*NIR may be one of the reasons dioxygen molecule can be observed in *Gt*NIR crystals. Recently reported oxygen-tolerant CuNIR from *Nitrosomonas europaea* (*Ne*NIR) does not lose the activity of nitrite reduction in the presence of oxygen [15]. This is because *Ne*NIR has a bulky and hydrophobic methionine residue in the middle of its substrate pocket, which makes a bottleneck preventing oxygen molecules from approaching the T2Cu site (Fig. S3). *Gt*NIR and other CuNIRs luck such a balky and hydrophobic residue at the corresponding position. Besides, *Gt*NIR has valine above the T2Cu site, whereas other CuNIRs have more bulky isoleucine at the same position (Fig. S3). As a result, *Gt*NIR has the widest substrate pocket in reported CuNIRs [14]. Therefore, dioxygen molecules can approach to T2Cu in *Gt*NIR more easily than in other CuNIRs.

It is obvious that dioxygen can bind to T2Cu in CuNIRs other than *Gt*NIR. Indeed, the reported NO-bound forms of CuNIR from *Achromobacter cycloclastes* (*Ac*NIR) [13] can also be refined as dioxygen bound forms. Interestingly, the used crystals in the experiment were not exposed either to NO_2^- or NO. Antonyuk *et al*. argues that observed molecules were endogenous NO; however, NO is an unstable and slightly soluble gas. Even if NO_2^-, from which NO can be produced by X-ray irradiation, was bound to T2Cu in the organism cells, it can be easily released during the purification and crystallization procedures because even chloride can bind to T2Cu in purification. Furthermore, the reported bond length between the N and O atoms in NO (1.41 Å in PDB code 2BW5) was significantly longer than the bond length of NO or NO^- (1.15 and 1.26 Å, respectively) [34] and more consistent with the bond length of dioxygen species.

Further investigations with several challenging techniques, such as Raman microspectroscopy and crystallization under anaerobic condition, are needed to confirm the present result and the precise state of the observed chemical species. We are preparing for those experiments.

Conflict of interest

The authors have no conflict of interest.

Acknowledgments

We thank Dr. K. Baba and Dr. N. Mizuno (beamline BL38B1 at SPring-8) for their support in microspectroscopic analysis and the data collection (2013A1592); and Dr. N. Matsugaki and Dr. Y. Yamada (beamline BL1A at Photon Factory) for their support in the data collection (2012R-78). Authors are grateful to Dr. S. Suzuki for discussion. Research reported in this publication was supported in part by a Grant-in-Aid for Japan Society for the Promotion of Science (JSPS) Fellows and JSPS KAKENHI. Grant Numbers: 254626 (to Y. F.); 24770096 (to E. M.); 25121719 and 25440022 (to H. M.); 24109017 and 25282230 (to T. I.).

Appendix A. Supplementary data

Supplementary data related to this article can be found at http://dx.doi.org/10.1016/j.bbrc.2015.07.025.

Transparency document

Transparency document related to this article can be found online at http://dx.doi.org/10.1016/j.bbrc.2015.07.025.

References

[1] W.G. Zumft, Cell biology and molecular basis of denitrification, Microbiol. Mol. Biol. Rev. 61 (1997) 533–616.
[2] J. Godden, S. Turley, D. Teller, E. Adman, M. Liu, W. Payne, J. LeGall, The 2.3 angstrom X-ray structure of nitrite reductase from Achromobacter cycloclastes, Science 253 (1991) 438–442.
[3] M.E.P. Murphy, S. Turley, E.T. Adman, Structure of nitrite bound to copper-containing nitrite reductase from Alcaligenes faecalis, J. Biol. Chem. 272 (1997) 28455–28460.
[4] F.E. Dodd, J.V. Beeumen, R.R. Eady, S.S. Hasnain, X-ray structure of a blue-copper nitrite reductase in two crystal forms. The nature of the copper sites, mode of substrate binding and recognition by redox partner, J. Mol. Biol. 282 (1998) 369–382.
[5] T. Inoue, M. Gotowda, Deligeer, K. Kataoka, K. Yamaguchi, S. Suzuki, H. Watanabe, M. Gohow, Y. Kai, Type 1 Cu structure of blue nitrite reductase from Alcaligenes xylosoxidans GIFU 1051 at 2.05 Å resolution: comparison of blue and green nitrite reductases, J. Biochem. 124 (1998) 876–879.
[6] T. Kakutani, T. Beppu, K. Arima, Regulation of nitrite reductase in the denitrifying bacterium Alcaligenes faecalis S-6, Agric. Biol. Chem. 45 (1981) 23–28.
[7] T. Kakutani, H. Watanabe, K. Arima, T. Beppu, A blue protein as inactivating factor for nitrite reductase from Alcaligenes faecalis strain S-6, J. Biochem. 89 (1981) 463–472.
[8] I.S. MacPherson, F.I. Rosell, M. Scofield, A.G. Mauk, M.E. Murphy, Directed evolution of copper nitrite reductase to a chromogenic reductant, Protein Eng. Des. Sel. 23 (2010) 137–145.
[9] R.W. Strange, F.E. Dodd, Z.H.L. Abraham, J.G. Grossmann, T. Brüser, R.R. Eady, B.E. Smith, S.S. Hasnain, The substrate-binding site in Cu nitrite reductase and its similarity to Zn carbonic anhydrase, Nat. Struct. Biol. 2 (1995) 287–292.
[10] R.W. Strange, L.M. Murphy, F.E. Dodd, Z.H.L. Abraham, R.R. Eady, B.E. Smith, S.S. Hasnain, Structural and kinetic evidence for an ordered mechanism of copper nitrite reductase, J. Mol. Biol. 287 (1999) 1001–1009.
[11] W.P. Michalski, D.J.D. Nicholas, Molecular characterization of a copper-containing nitrite reductase from Rhodopseudomonas sphaeroides forma sp. denitrificans, Biochim. Biophys. Acta 828 (1985) 130–137.
[12] E.I. Tocheva, F.I. Rosell, A.G. Mauk, M.E. Murphy, Side-on copper-nitrosyl coordination by nitrite reductase, Science 304 (2004) 867–870.
[13] S.V. Antonyuk, R.W. Strange, G. Sawers, R.R. Eady, S.S. Hasnain, Atomic resolution structures of resting-state, substrate- and product-complexed Cu-nitrite reductase provide insight into catalytic mechanism, Proc. Natl. Acad. Sci. U. S. A. 102 (2005) 12041–12046.
[14] Y. Fukuda, K.M. Tse, M. Lintuluoto, Y. Fukunishi, E. Mizohata, H. Matsumura, H. Takami, M. Nojiri, T. Inoue, Structural insights into the function of a thermostable copper-containing nitrite reductase, J. Biochem. 155 (2014) 123–135.
[15] T.J. Lawton, K.E. Bowen, L.A. Sayavedra-Soto, D.J. Arp, A.C. Rosenzweig, Characterization of a nitrite reductase involved in nitrifier denitrification, J. Biol. Chem. 288 (2013) 25575–25583.
[16] N. Shimizu, T. Shimizu, S. Baba, K. Hasegawa, M. Yamamoto, T. Kumasaka, Development of an online UV-visible microspectrophotometer for a macromolecular crystallography beamline, J. Synch. Rad. 20 (2013) 948–952.
[17] K.S. Paithankar, E.F. Garman, Know your dose: RADDOSE, Acta Cryst. D. 66 (2010) 381–388.
[18] Z. Otwinowski, W. Minor, Processing of X-ray diffraction data collected in oscillation mode, Methods Enzymol. 276 (1997) 307–326.
[19] A. Vagin, A. Teplyakov, Molecular replacement with MOLREP, Acta Cryst. D 66 (2010) 22–25.
[20] M.D. Winn, C.C. Ballard, K.D. Cowtan, E.J. Dodson, P. Emsley, P.R. Evans, R.M. Keegan, E.B. Krissinel, A.G. Leslie, A. McCoy, S.J. McNicholas, G.N. Murshudov, N.S. Pannu, E.A. Potterton, H.R. Powell, R.J. Read, A. Vagin, K.S. Wilson, Overview of the CCP4 suite and current developments, Acta Cryst. D 67 (2011) 235–242.
[21] G.N. Murshudov, P. Skubak, A.A. Lebedev, N.S. Pannu, R.A. Steiner, R.A. Nicholls, M.D. Winn, F. Long, A.A. Vagin, REFMAC5 for the refinement of macromolecular crystal structures, Acta Cryst. D. 67 (2011) 355–367.
[22] P. Emsley, B. Lohkamp, W.G. Scott, K. Cowtan, Features and development of Coot, Acta Cryst. D 66 (2010) 486–501.
[23] V.B. Chen, W.B. Arendall 3rd, J.J. Headd, D.A. Keedy, R.M. Immormino, G.J. Kapral, L.W. Murray, J.S. Richardson, D.C. Richardson, MolProbity: all-atom structure validation for macromolecular crystallography, Acta Cryst. D. 66 (2010) 12–21.
[24] L.B. LaCroix, S.E. Shadl, Y. Wang, B.A. Averill, B. Hedman, K.O. Hodgson, E.I. Solomon, Electronic structure of the perturbed blue copper site in nitrite reductase: spectroscopic properties, bonding, and implications for the entatic/rack state, J. Am. Chem. Soc. 118 (1996) 7755–7768.
[25] J. Yano, J. Kern, K.D. Irrgang, M.J. Latimer, U. Bergmann, P. Glatzel, Y. Pushkar, J. Biesiadka, B. Loll, K. Sauer, J. Messinger, A. Zouni, V.K. Yachandra, X-ray damage to the Mn_4Ca complex in single crystals of photosystem II: a case study for metalloprotein crystallography, Proc. Natl. Acad. Sci. U. S. A. 102 (2005) 12047–12052.
[26] T. Beitlich, K. Kuhnel, C. Schulze-Briese, R.L. Shoeman, I. Schlichting, Cryoradiolytic reduction of crystalline heme proteins: analysis by UV–Vis spectroscopy and X-ray crystallography, J. Synch. Rad. 14 (2007) 11–23.
[27] E.I. Tocheva, F.I. Rosell, A.G. Mauk, M.E.P. Murphy, Stable copper-nitrosyl formation by nitrite reductase in either oxidation state, Biochemistry 46 (2007) 12366–12374.

[28] M.A. Hough, S.V. Antonyuk, R.W. Strange, R.R. Eady, S.S. Hasnain, Crystallography with online optical and X-ray absorption spectroscopies demonstrates an ordered mechanism in copper nitrite reductase, J. Mol. Biol. 378 (2008) 353–361.
[29] K. Fujisawa, M. Tanaka, Y. Moro-oka, N. Kitajima, A monomeric side-on superoxocopper(II) complex: $Cu(O_2)(HB(3\text{-}tBu\text{-}5\text{-}iPrpz)_3)$, J. Am. Chem. Soc. 116 (1994) 12079–12080.
[30] S. Itoh, Mononuclear copper active-oxygen complexes, Curr. Opin. Chem. Biol. 10 (2006) 115–122.
[31] A. Kunishita, M.Z. Ertem, Y. Okubo, T. Tano, H. Sugimoto, K. Ohkubo, N. Fujieda, S. Fukuzumi, C.J. Cramer, S. Itoh, Active site models for the Cu(A) site of peptidylglycine alpha-hydroxylating monooxygenase and dopamine beta-monooxygenase, Inorg. Chem. 51 (2012) 9465–9480.
[32] C.J. Cramer, W.B. Tolman, Mononuclear $Cu\text{-}O_2$ complexes: geometries, spectroscopic properties, electronic structures, and reactivity, Acc. Chem. Res. 40 (2007) 601–608.
[33] Y. Fukuda, H. Koteishi, R. Yoneda, T. Tamada, H. Takami, T. Inoue, M. Nojiri, Structural and functional characterization of the Geobacillus copper nitrite reductase: involvement of the unique N-terminal region in the interprotein electron transfer with its redox partner, Biochim. Biophys. Acta 1837 (2014) 396–405.
[34] J.A. McCleverty, Chemistry of nitric oxide relevant to biology, Chem. Rev. 104 (2004) 403–418.